

Distribution Transformer Modelling: Accounting for Non-Linearities Resulting From Higher Harmonic Loads

WI4204 - Advanced Modelling

Final Report

Delft University of Technology

Faculty of Electrical Engineering, Mathematics and Computer Science

Supervisor: Dr. Domenico Lahaye

Philip Soliman (4945255), Auke Schaap (4457919)

June 17, 2023

Abstract

Due to the wide adoption of solar panels, electric vehicles, and other technologies, the energy supply and consumption in Netherlands has changed drastically. This has led to a change in the load profile of the distribution transformers, which are used to step down the voltage from the medium voltage grid to the low voltage grid. Currently, models do not accurately reflect the behaviour of the transformers under these new conditions. This paper presents a model that can accurately model the magnetic field without assuming a sinusoidal solution. The model can be used to model any frequency, as well as multiple frequencies. The model also correctly captures the behaviour of the core at loads close to the saturation point, by including the non-linear permeability of the core material. These are both improvements over the current linear models, which are not able to capture these behaviours. Future improvements include an even finer mesh to capture the skin effect even better and improvements to the non-linear algorithm to reduce the computation time.

Chapter 1

Introduction

Over the last few years, the energy supply and consumption in the Netherlands has changed drastically. For example, there has been an increase in energy generated by solar panels, as well as an increase in the number electric vehicles on roads van Dijk et al., 2022. Both the solar panels on people's roofs as well the charging docks for their electric vehicles introduce higher harmonics into the electricity grid N.V., 2021, Sugiyama, 2012. These higher harmonics increase the load on distribution transformers, which causes overheating, degraded performance and decreased lifetime van Dijk et al., 2022

Distribution transformers are used to transform the high voltage electricity from the transmission grid to a lower voltage for the end-user. In this process, some of the electrical potential energy is dissipated as heat.

In modelling these losses, we can assume the magnetic field in the core to have the same temporal behavior as the the load on the transformer; sinusoidal with the same frequency. This works for load profiles with multiple frequencies, as long as the magnetic permeability of the core is assumed constant.

However, the magnetic permeability μ of the core is only constant by approximation. In reality μ depends on the magnetic field strength, which introduces non-linearities in the governing equations. For low harmonics, i.e. 50 Hz, these non-linearities are negligible. For higher harmonics, the skin-effect causes the magnetic flux to be concentrated near the edges of the transformer. The flux in these edge regions is then high enough that μ can no longer be assumed to be constant. This results in a model error for higher harmonics.

Additionally, the superposition of the magnetic field resulting from several load frequencies is no longer valid for non-linear systems. This is because each of the frequencies are now coupled to each other, through μ 's dependence on the magnetic field strength.

This paper aims to model the magnetic field in a distribution transformer, taking into account the non-linearities introduced by higher frequencies and loads. The proposed model makes no assumptions on the frequency of the magnetic field resulting from a load profile containing (multiple) higher harmonics.

Chapter 2 explains relevant background information. In chapter 3, the model is derived. Then, chapter 4 presents the results of the model. Lastly, chapter 5 discusses the results and the model.

The code used to generate the results can be found at <https://github.com/aukeschaap/am-transformers>.

Chapter 2

Background

This chapter provides some background theory on the problem. It describes the electrical grid, the function of a transformer, the effect of modern appliances on the transformer and modelling of this effect. It draws heavily from the work of van Dijk et al., 2022.

2.1 Electrical grid

Power generated at dams, nuclear power- and coal plants is transmitted to the consumer through the electrical grid. The grid is a network of power lines, transformers and other equipment. The grid is divided into three parts: generation, transmission and distribution. All these components are displayed in figure 2.1.

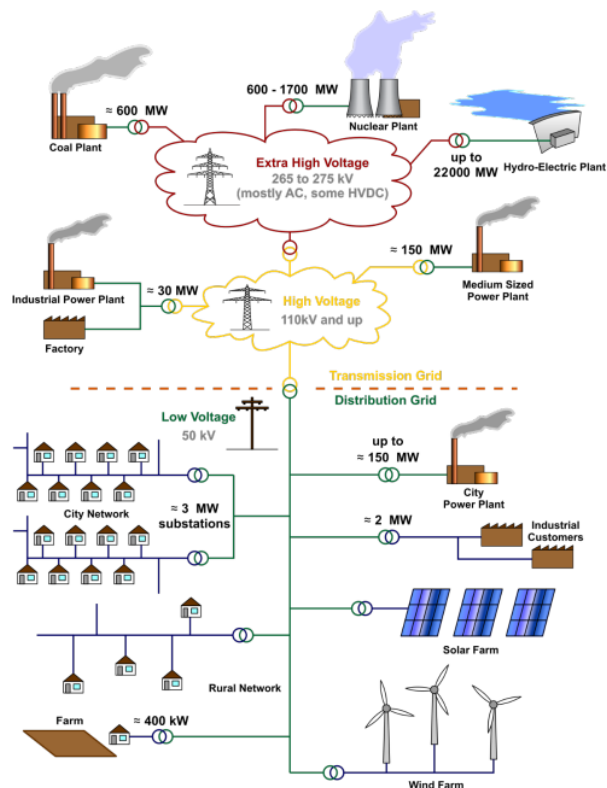


Figure 2.1: Electricity grid Bizon, 2010.

In the Netherlands specifically, the grid is divided into three voltage levels: extra high voltage, high voltage and low voltage. The transmission grid ensures this high voltage ends

up at factories, large power transformers and additional power is extracted from industrial and medium sized power plants. Moreover, it is managed by a Transmission System Operator (TSO).

Similarly, the distribution grid connects the transmission grid, cities, the rural network, solar-, wind farms to each other. It, in turn is managed by a Distribution System Operator (DSO) In this paper the focus is on the transformers in the distribution grid. Figure 2.2 shows an example of such an transformer. This is because the distribution grid is the last part of the grid before the consumer. Consequently, the effects of modern appliances are most prominent in these types of transformers.



Figure 2.2: Transformer Gebouwd, 2008

The main goal of any transformer is to allow for the transmission of electrical energy over long distances. It achieves this by either increasing or decreasing voltage. In the former case, it is called a step-up transformer, in the latter case a step-down transformer. A step-up transformer allows for long distance transmission of electrical energy because the power loss is proportional to the current squared, which is decreased for increased voltage. On the other hand, a step-down transformer is used to decrease the voltage to a level that is safe for the end-consumer.

2.2 Workings of transformer

A transformer is a device that transfers electrical energy from one circuit to another through inductively coupled conductors. It has three main components: a primary coil, a secondary coil and a core (see Figure 2.3). The primary coil is connected to the source of the electrical energy, the secondary coil is connected to a load and the core is made from a ferromagnetic material. In the case of a distribution transformer, the primary coil is connected to the transmission grid and the secondary coil is connected to the distribution grid.



Figure 2.3: Main components of a transformer: primary (outer) coil, secondary (inner) coil and core. The coils are wound around the core and are wrapped in insulation themselves (Satsangi, 2014).

The insulation around the coils is necessary to prevent short-circuiting. Hence the lifetime of a transformer is limited by the lifetime of the insulation. The latter in turn is determined by the amount of heat generated in the transformer. This heat is dissipated through the core and the coils, where the core is the main contributor. Therefore, this paper focusses on modelling the magnetic field generated in the core. The core losses and subsequent temperature profile may then be calculated from this magnetic field using the Steinmetz equation (Sudhoff, 2014; van Dijk et al., 2022).

2.3 Higher Harmonics

As stated in Section 2.1, the effect of modern appliances like computers, LEDs, solar panels and electric cars is most prominent in the distribution grid. LEDs, for instance, are non-linear loads, which means they draw a current that is composed of a fundamental frequency and higher harmonics. These higher harmonics are multiples of the fundamental frequency. The effect of these higher harmonics is that the current is no longer sinusoidal, but has a distorted shape. This distortion is shown in Figure 2.4.

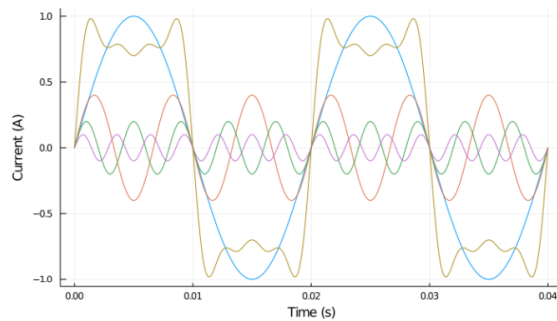


Figure 2.4: Distorted current waveform (van Dijk et al., 2022).

The magnetic field in the core depends on the frequency. A concrete example of this is the skin effect, which is the tendency of an alternating electric current to become distributed within a conductor such that the current density is largest near the surface of the conductor, and decreases with greater depths in the conductor. The depth at which the current density is 37% of the current density at the surface is called the skin depth. It is given by (Van der Vorst

Frequency	δ (mm)
50 Hz	0.701 mm
100 Hz	0.496 mm
150 Hz	0.351 mm
500 Hz	0.222 mm
1000 Hz	0.157 mm

Table 2.1: Numerical values for the skin effect at different frequencies, with parameters as described below.

et al., 2007)

$$\delta = \sqrt{\frac{2\rho}{\omega\mu}} = \sqrt{\frac{\rho}{\pi f \mu_0 \mu_r}}, \quad (2.1)$$

where:

- ρ : The resistivity of the conductor. For an iron core, this is taken as $\rho = 9.71 \cdot 10^{-8} \Omega \cdot \text{m}$ (Giancoli, 1995).
- μ : The permeability of the conductor, given by $\mu_r \mu_0$.
- μ_r : The relative magnetic permeability of the conductor. For an iron core, this is somewhere around 10^3 . Therefore, this is chosen as $\mu_r = 1000$.
- μ_0 : The permeability of free space. This is generally taken as $\mu_0 = 4\pi \cdot 10^{-7} \text{ H/m}$.
- ω : The angular frequency of current, given by $2\pi f$, where f is the frequency. This is variable in our case.

This becomes smaller for higher frequencies, and is hence more prominent for higher harmonics. Therefore, higher harmonics lead to an increased core loss. A numerical result is given in table 2.1.

2.4 Permeability of the core

Another complication in modelling the magnetic field in the core is that the permeability of the core is not constant for sufficiently large magnetic fields. This is called the saturation of the core. The permeability of the core is given by

$$\mu = \mu_0 \mu_r, \quad (2.2)$$

where μ_0 is the permeability of free space and μ_r is the relative permeability of the core. The permeability is a function of the magnetic field strength H . The magnetic field strength is given by

$$H = \frac{B}{\mu}, \quad (2.3)$$

where B is the magnetic flux density.

From this it follows that we can derive μ given we know the relation between B and H . This relation is called the B-H curve, an example of which is visible in Figure 2.5.

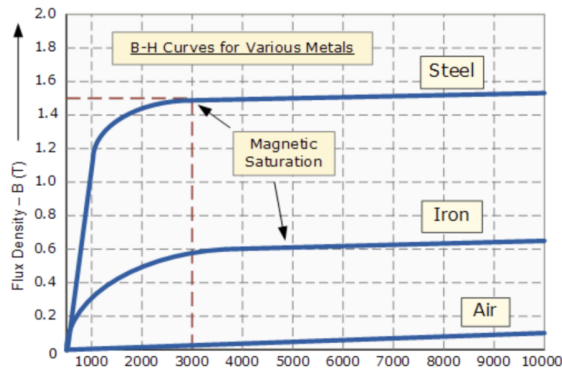


Figure 2.5: B-H curve for various metals. μ is the slope of this curve. Once μ becomes nearly zero, the material is said to be the saturated unknown, 2013.

Chapter 3

Model

This chapter describes the model used to simulate the magnetic field in the transformer core. The implementation is available at <https://github.com/aukeschaap/am-transformers>.

3.1 Problem derivation

To define the problem, we start with the Maxwell equations and corresponding constitutive relations. The Maxwell equations are given by

$$\begin{aligned}\nabla \times \mathbf{E} &= -\frac{\partial \mathbf{B}}{\partial t}, \\ \nabla \times \mathbf{H} &= \mathbf{J} + \frac{\partial \mathbf{D}}{\partial t}, \\ \nabla \cdot \mathbf{B} &= 0, \\ \nabla \cdot \mathbf{D} &= \rho,\end{aligned}$$

where

- \mathbf{E} , [V/m] is the electric field intensity,
- \mathbf{H} , [A/m] is the magnetic field intensity,
- \mathbf{J} , [A/m²] is the current density,
- \mathbf{B} , [T] is the magnetic flux density,
- \mathbf{D} , [C/m²] is the electric flux density,
- ρ , [C/m³] is the free charge density.

These have the following constitutive relations:

$$\begin{aligned}\mathbf{J} &= \mathbf{J}_e + \mathbf{J}_c \\ \mathbf{B} &= \mu \mathbf{H} \\ \mathbf{J}_c &= \sigma \mathbf{E} \\ \mathbf{D} &= \epsilon \mathbf{E}\end{aligned}$$

where

- \mathbf{J}_e is the external current density,
- \mathbf{J}_c is the conduction current density,

- σ is the conductivity of the material,
- $\mu = \mu_0\mu_r$ is the permeability of the core,
- $\epsilon = \epsilon_0\epsilon_r$ is the permittivity of the material.

Assumption. The permittivity of vacuum ϵ_0 is very small, ($\mathcal{O}(10^{-12})$), and for all materials in this research $\epsilon_r < 10$, so ϵ can be neglected. Therefore, $\mathbf{D} \approx 0$ and can be neglected.

Substituting this in the Maxwell equations yields three equations,

$$\begin{aligned}\nabla \times \mathbf{E} &= -\frac{\partial \mathbf{B}}{\partial t}, \\ \nabla \times [\mu^{-1} \mathbf{B}] &= \mathbf{J}_e + \sigma \mathbf{E}, \\ \nabla \cdot \mathbf{B} &= 0.\end{aligned}$$

Using the potential formulation,

$$\begin{aligned}\mathbf{E} &= -\nabla \varphi - \frac{\partial \mathbf{A}}{\partial t}, \\ \mathbf{B} &= \nabla \times \mathbf{A},\end{aligned}$$

we can formulate a system that we can solve.

Assumption. We assume that the contribution of the electrostatic field φ is negligible compared to the contribution of the potential field \mathbf{A} . That is, $\nabla \varphi = 0$, which implies that $\mathbf{E} = -\frac{\partial \mathbf{A}}{\partial t}$.

Assumption. The flow of current is oriented along the z axis, and the geometry is in the xy plane. That is, $\mathbf{A} = (0, 0, A_z)$ and $\mathbf{J}_e = (0, 0, J_z)$. This implies $\nabla \times \mathbf{A} = (\partial_y A_z, -\partial_x A_z, 0)$.

Substituting these assumptions into the Maxwell equations and rearranging, we obtain our problem definition.

$$\sigma \frac{\partial A_z}{\partial t} = - \left(\frac{\partial}{\partial x} \left[\frac{1}{\mu} \frac{\partial A_z}{\partial x} \right] + \frac{\partial}{\partial y} \left[\frac{1}{\mu} \frac{\partial A_z}{\partial y} \right] \right) + J_z,$$

Problem Definition. Find A_z in the system

$$\sigma \frac{\partial A_z}{\partial t} = -\nabla \cdot \left(\frac{1}{\mu} \nabla A_z \right) + J_z, \quad (3.1)$$

where

- A_z is the magnetic vector potential in the z direction,
- μ is the permeability of the core,
- J_z is the imposed source current density,
- σ is the conductivity of the core.

From this point onwards, this will be formulated as

$$\sigma \dot{u} = \nabla \cdot \left[\frac{1}{\mu} \nabla u \right] + f. \quad (3.2)$$

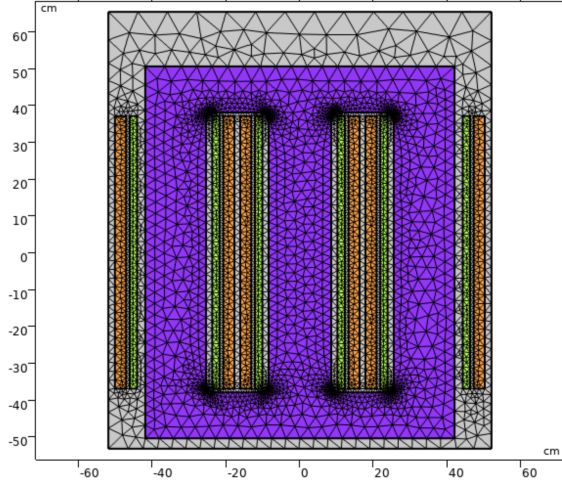


Figure 3.1: The mesh used to discretize the domain (van Dijk et al., 2022).

3.2 Spatial discretisation using finite element method

To solve this system, the finite element method can be used. Choosing a first order basis function

$$\phi_i = a_i + b_i x + c_i y,$$

for each node i , the solution u can be approximated as

$$u = \sum_{i=1}^N u_i \phi_i.$$

This results in the following weak form.

Weak Form.

$$\sigma M \dot{u} = K(\mu(u))u + f, \quad (3.3)$$

where

u is A_z , the solution.

- M is the mass matrix,
- K is the stiffness matrix,
- f is the source term, given by J_z ,

The mass matrix on element e_k , M_{e_k} is given by

$$M_{e_k} = \left[\int_{\Omega_{e_k}} \phi_i \phi_j d\Omega \right]_{1 \leq i,j \leq 3}$$

Similarly, the local stiffness matrix K_{e_k} is given by

$$\begin{aligned} K_{e_k}(\mu(u)) &= \left[\int_{\Omega_{e_k}} \phi_i \nabla \cdot \left(\frac{1}{\mu} \nabla \cdot \phi_j \right) d\Omega \right]_{1 \leq i,j \leq 3} \\ &= - \int_{\Omega_{e_k}} \frac{1}{\mu} \nabla \phi_i \nabla \phi_j d\Omega \end{aligned}$$

Similarly the local source term f_{e_k} is given by

$$f_{e_k}(t) = \left[\int_{\Omega_e} f(x, y, t) \phi_i d\Omega \right]_{1 \leq i \leq 3}$$

We can exactly calculate the integrals using the following quadrature rule for first order polynomials.

$$\int_{\Omega_e} g(x, y) dx dy = A_{e_k} \bar{g}_{e_k},$$

where A_{e_k} is the area of element e_k and \bar{g}_{e_k} is the average of function g over element e_k .

3.2.1 Time dependence

If μ is constant we may write $K(\mu(u)) = K(\mu) = \frac{1}{\mu}K$. In this case the use of separation of variables is valid. If μ is dependent on u , separation of variables is not valid due to the non-linear nature of the problem. In this case a time stepping method is necessary. This section outlines both approaches and their implementation. Ultimately, the time stepping method is used, because the permeability this paper is concerned with the non-linear case.

3.2.2 Separation of variables

Applying separation of variables

$$u(x, y, t) = \hat{u}(x, y) \cdot e^{j\omega t}.$$

to the weak form (3.3) yields

$$\left[\sigma \omega j M + \frac{1}{\mu} A \right] \hat{u} = \hat{f}.$$

This is a linear system of equations, which can be solved using a linear solver. Additionally it may be solved for multiple frequencies $\omega_1, \omega_2, \dots$ by writing

$$u(x, y, t) = \hat{u}_1(x, y) e^{j\omega_1 t} + \hat{u}_2(x, y) e^{j\omega_2 t} + \dots, \quad (3.4)$$

solving the above system for each frequency, and summing the solutions. However it must be noted that the influence of the frequencies on each other is not taken into account in this approach. This is why the time stepping method is used in this paper.

3.2.3 Time stepping

The time derivative in equation 3.3 can be approximated using a backward Euler method,

$$\sigma M \frac{u^k - u^{k-1}}{\Delta t} = K(u^k)u^k + f^k,$$

where u^k is the solution at time t^k and u^{k+1} is the solution at time $t^{k+1} = t^k + \Delta t$. This leads to the following implicit time stepping scheme.

$$\left[\sigma M - \Delta t K(u^{k-1}) \right] u^k = \sigma M u^{k-1} + \Delta t f^k.$$

During each time step, this non-linear system of equations must be solved. This is done using an iterative scheme with dampening factor α . This means that instead of u_i^k , there is \tilde{u}_i^k , defined by

$$\tilde{u}_i^k = \alpha \tilde{u}_{i-1}^k + (1 - \alpha) u_{i-1}^k,$$

where the superscript k denotes time, and subscript i denotes the iteration number. This is then used for solving the system of equations for u_i^k :

$$[\sigma M - \Delta t K(\tilde{u}_i^k)] u_i^k = [\sigma M \tilde{u}_i^k + \Delta t f^k]. \quad (3.5)$$

This is repeated until the residual is sufficiently small. That is

$$\|u_{i-1}^k - u_i^k\|_2 \leq \epsilon,$$

where ϵ is a small number. In this paper $\epsilon = 10^{-3}$ is used. The full algorithm is given in Algorithm 1.

Algorithm 1 Time-stepping algorithm using Backward Euler

```

1: function NONLINEAR-SOLVE
2:    $u^0 \leftarrow \mathbf{0}$ 
3:   for  $k \in [0, N_t]$  do
4:      $i \leftarrow 0$ 
5:      $u_0^k \leftarrow u^{k-1}$ 
6:      $\tilde{u}_0^k \leftarrow u^{k-1}$ 
7:     while  $\Delta u \leq \epsilon$  do
8:        $i \leftarrow i + 1$ 
9:        $\tilde{u}_i^k \leftarrow \alpha \tilde{u}_{i-1}^k + (1 - \alpha) u_{i-1}^k$ 
10:       $u_i^k \leftarrow [\sigma M - \Delta t K(\tilde{u}_i^k)]^{-1} [\sigma M \tilde{u}_i^k + \Delta t f^k]$ 
11:       $\Delta u \leftarrow \|u_{i-1}^k - u_i^k\|_2$ 
12:    end while
13:     $u^{k+1} \leftarrow u_i^k$ 
14:  end for
15: end function

```

Chapter 4

Results

In this chapter we present the results of open-circuit simulations of the digital transformer. An open circuit of a transformer is of particular interest, as it is generally used to determine core losses. We run the simulations for both the linear- as well as the non-linear model. All simulations are run with

- $I_s = 777.72 \text{ A}$,
- $I_p = 0 \text{ A}$,
- $N_s = 266$,
- $N_p = 6$,
- $f = 50 \text{ Hz}$.

These are the parameters used in van Dijk et al., 2022.

4.1 Linear behaviour

Taking $\mu_{r,core} = 1000 \frac{\text{H}}{\text{m}}$ and $\mu_{r,air} = 10 \frac{\text{H}}{\text{m}}$, fig. 4.1 shows the magnetic flux through all three core legs for three periods of the source signal. This can be viewed as the superposition of three contributions, one for each core leg

$$\begin{aligned} B_{\text{left leg}} &= B_0 (\sin(\omega t - \phi) - \sin(\omega t)) , \\ B_{\text{middle leg}} &= B_0 (\sin(\omega t) - \sin(\omega t - \phi) - \sin(\omega t + \phi)) , \\ B_{\text{right leg}} &= B_0 (\sin(\omega t + \phi) - \sin(\omega t)) , \end{aligned}$$

where B_0 is the amplitude of the magnetic flux and ϕ is the phase shift of the three-phase source signal. Note that this is only true for the linear model. The above equations are derived by realising that any coil induces a magnetic flux in the core leg it is wrapped around and an opposing flux in its neighbouring legs. Plotting above expressions gives fig. 4.2. Comparing this to fig. 4.1, it is clear that the linear model behaves as expected.

4.2 Non-linear behaviour

We now take

$$\mu_{\text{core, r}}(||\mathbf{B}||) = \left(\alpha + (1 - \alpha) \frac{||\mathbf{B}||^{2\beta}}{||\mathbf{B}||^{2\beta} + \gamma} \right)^{-1},$$

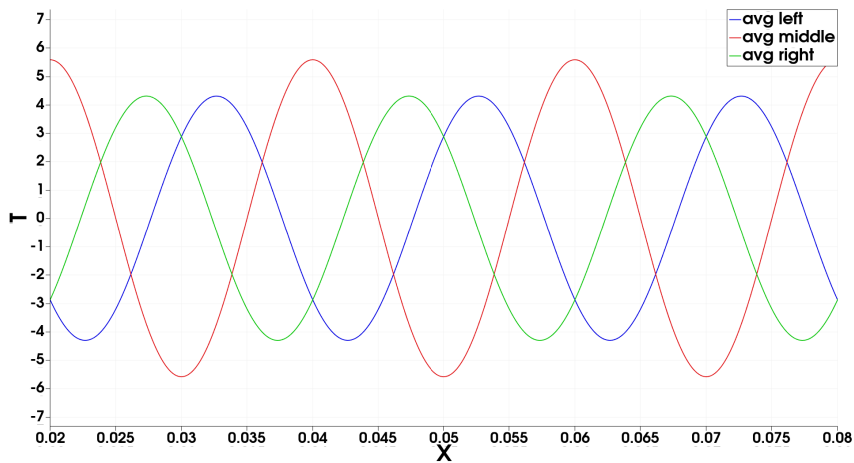


Figure 4.1: Magnetic flux against time in all three core legs for the linear model.

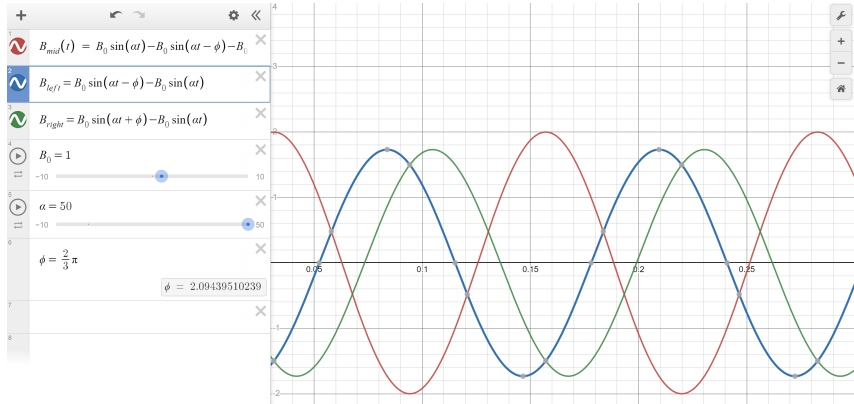


Figure 4.2: Predicted magnetic flux against time in all three core legs for the linear model.

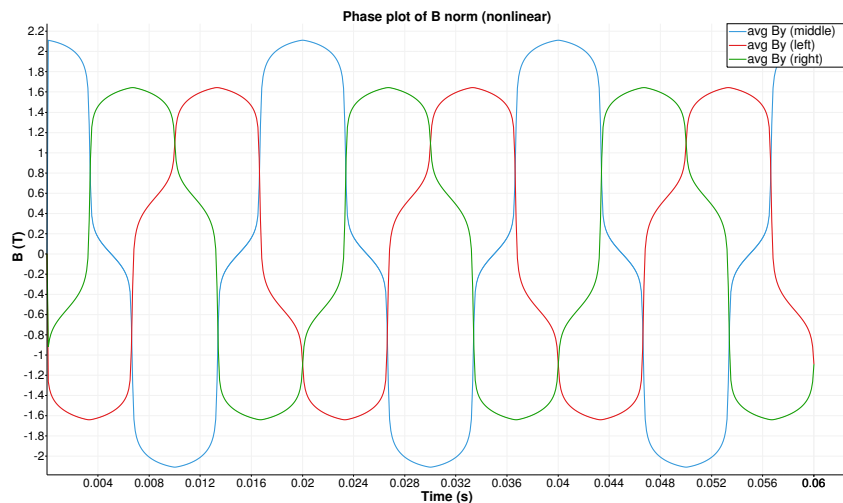


Figure 4.3: Phase plot of B for the non-linear model.

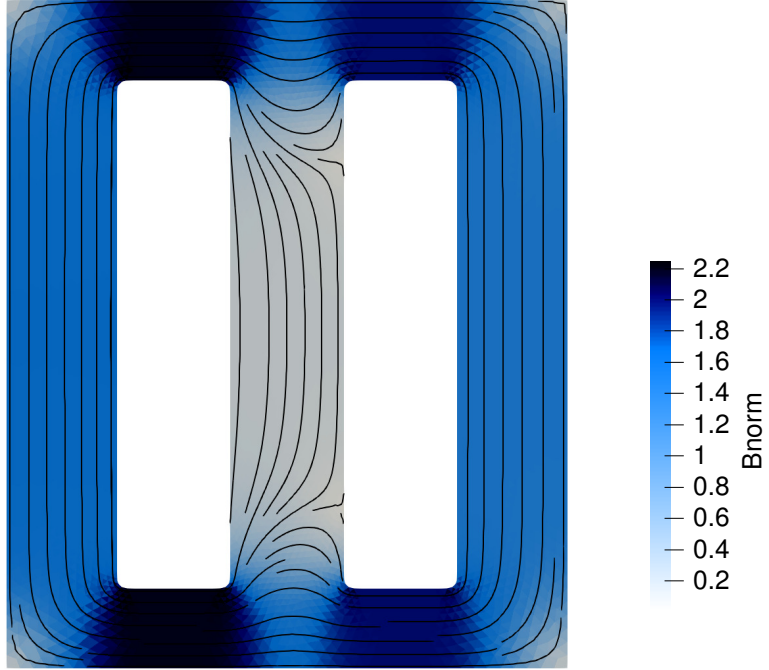


Figure 4.4: $\|B\|$ at $t = 0.004$ s for the non-linear model.

$\alpha = 2.12 \times 10^{-4}$, $\beta = 7.358$ and $\gamma = 1.18 \times 10^{-4}$. which has a saturation point at $\|\mathbf{B}\| \approx 2$ T. fig. 4.3 shows the phase plot of B for the non-linear model, which is quite different from the linear case.

Firstly, the magnetic flux rises much more sharply than in the linear case. This is expected, as the permeability of the core is higher than in the linear case because the core is unsaturated.

Secondly, the maximum magnetic flux is much lower than in the linear case, ≈ 2 T vs. ≈ 6 . This behaviour is also expected, as the saturation point of the core is reached, which means that the permeability of the core is much lower than in the linear case. This influences the magnetic flux, and is correctly captured by the non-linear model. This is visible in the plot by the quick flattening of the magnetic flux at e.g. 2 Tesla for the middle leg.

The full solution for the magnetic flux in all three core legs is shown in Figure 4.4. If we compare this with fig. 4.5, we can interpret the differences between the models. One of the implications of the lower permeability, is that the flux can not penetrate that area of the core. In fig. 4.5 it can be seen that the flux rises to 12 Tesla near the inside corners; this is unrealistic. In the non-linear model, this is not the case. However, other parts of the iron core are still permeable, and therefore the flux can still penetrate there. This leads to nearly full saturation of the core at the cross-sections. This is much more realistic behaviour.

This hypothesis can be confirmed by looking at a plot of the permeability, given in fig. 4.6. The permeability is very high at the points where the flux is high, and low where the flux is low. This is exactly what we expect from the non-linear model.

As a last test, we can look at the permeability as a function of the magnetic flux, given in fig. 4.7. This is a plot of the permeability as a function of $\|B\|$. We see that the permeability is very high for low values of $\|B\|$, and then drops off quickly, as expected.

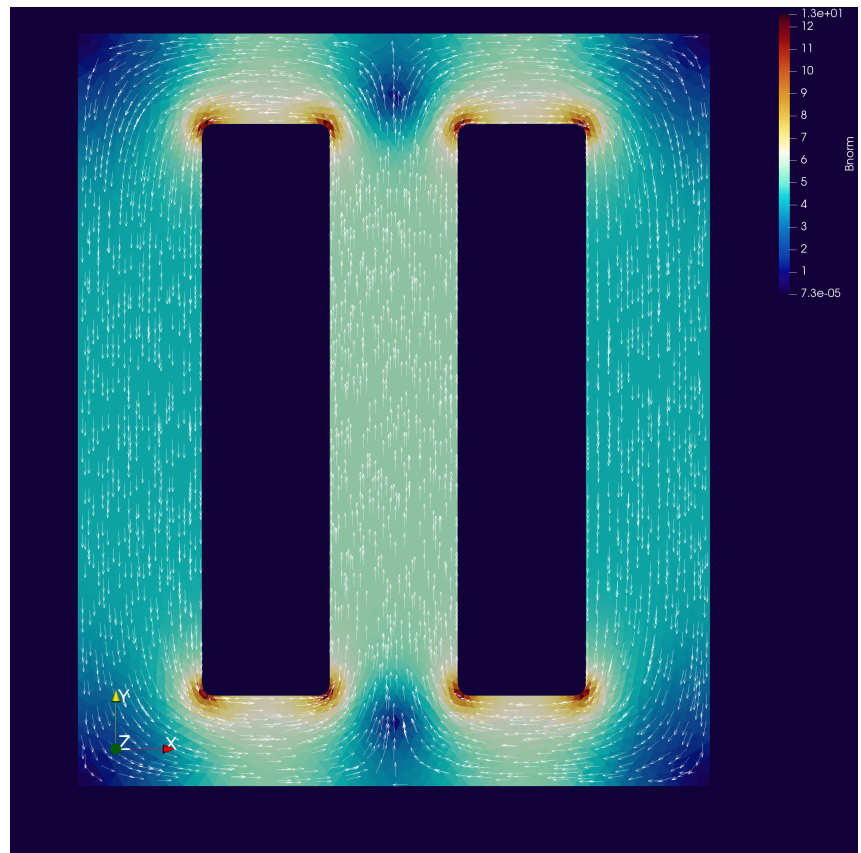


Figure 4.5: $\|B\|$ at $t = 0.004$ s, for the linear model.

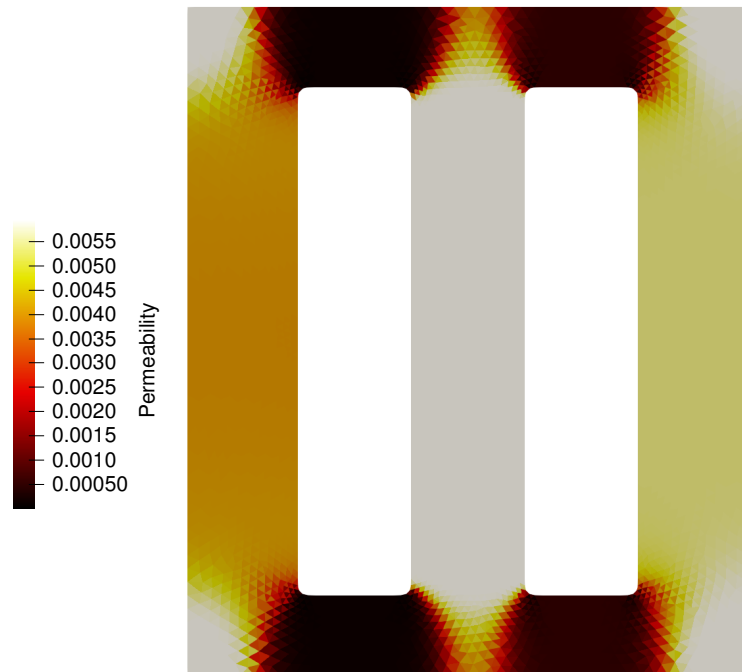


Figure 4.6: Permeability of the core at $t = 0.004$ s, for the non-linear model.

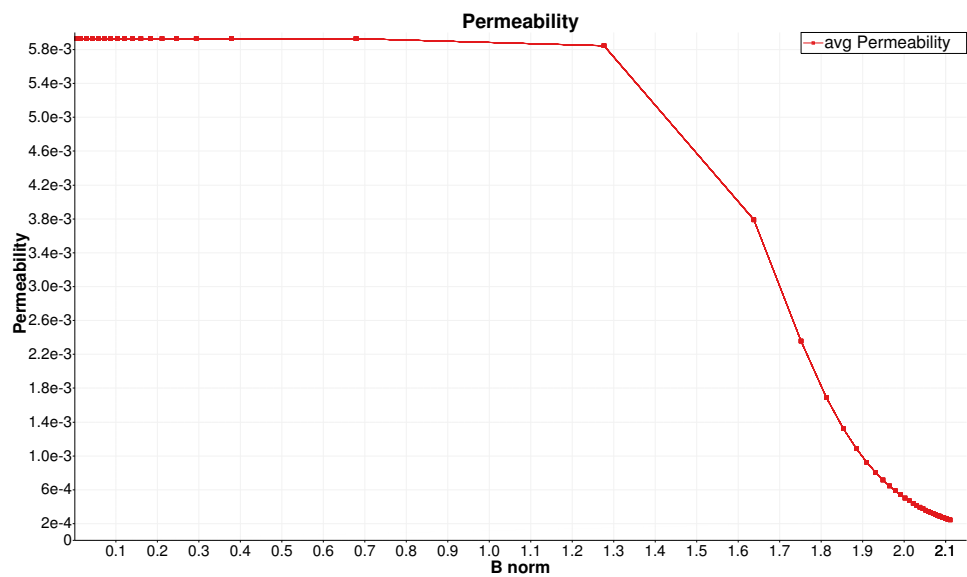


Figure 4.7: Permeability as a function of $\|B\|$.

Chapter 5

Discussion

5.1 Conclusion

From the results presented in chapter 4, we can conclude the following.

Firstly, the method is able to model the transformer core in a way that is consistent with the physical properties of the core material. This is shown by the fact that the magnetic flux density in the core is inversely proportional to the permeability of the core material. Consequently, the model correctly captures the behaviour of the core at loads close to the saturation point, as seen by the fact that the magnetic flux density in the core is constant across the cross section of the core. This directly shows that the linear model is not able to capture the behaviour of the core at loads close to the saturation point.

Furthermore, this model does not make any assumptions on the underlying frequency of the magnetic vector potential. As a result, the model can also be easily adapted to model higher and multiple frequencies, as well as multiple frequencies, correctly. As the non-linearities disallow separation of variables in the frequency domain, this is an improvement over the previous work.

5.2 Future work

The model presented in this paper is a first step towards a more accurate model of the magnetic field in a distribution transformer. However, there are still some improvements that can be made.

This paper only presents results for a single frequency. In theory, the model is also valid for higher, as well as multiple frequencies. However, the model is not yet validated for these cases. Therefore, more research is needed to determine the validity of the model for these cases.

At this moment, the model is not fully optimized. As a result, the execution time is quite long. If this is to be used to model a longer time horizon, the execution time needs to be reduced. Some steps in this direction have already been taken:

- Matrices have been implemented in a sparse format, which reduces the memory usage and the number of operations needed to perform the matrix-vector multiplications.
- A data structure `FastSparse` has been implemented, that efficiently allocates memory for initializing the (sparse) matrices M and K .
- The assembly of the matrices M and K has been optimized to use to least amount of memory allocations possible.

However, there are still some steps that can be taken to further reduce the execution time:

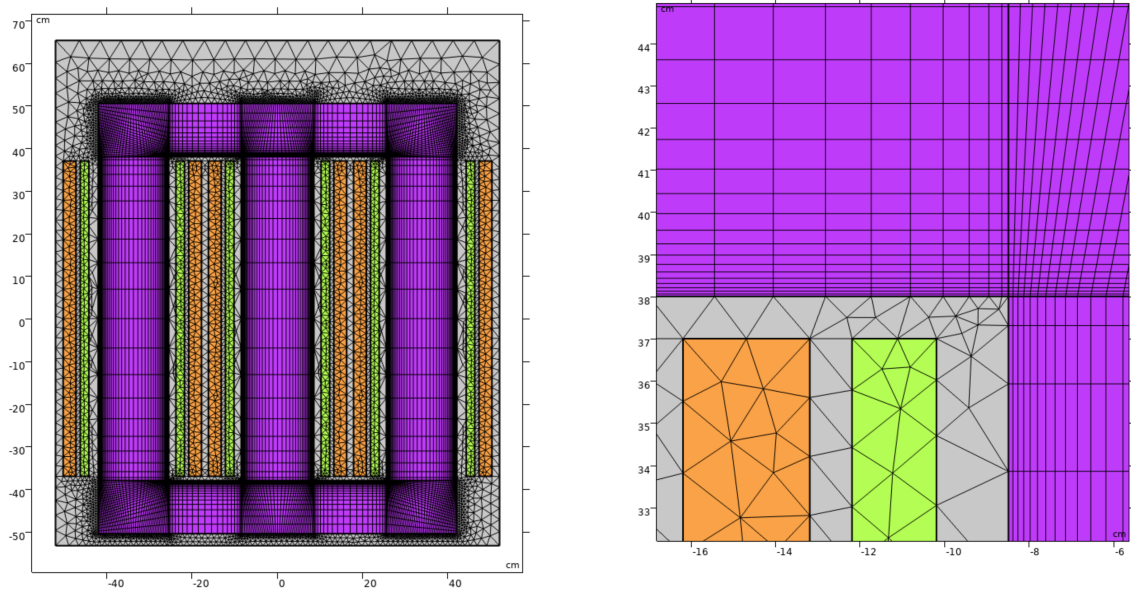


Figure 5.1: Hybrid mesh that can be used to accurately model the skin effect (van Dijk et al., 2022).

- Efficient linear system solver: the current linear system solver is not very efficient. This could be an iterative method, or a Krylov subspace method.
- Backward Euler is used to time-step. This could be done more accurately by using a higher order method, such as the Runge-Kutta method, further improving execution time.

Furthermore, the parameters used in the model are not in agreement with reality. For instance, the core does not operate close to saturation in reality, but at much lower flux densities. Most parameters are estimated based on van Dijk et al., 2022, and might therefore not be accurate. More research is needed to determine the correct parameters.

Finally, the mesh used in this paper can be improved. The mesh used in this paper is a triangular mesh, and lacks detail to correctly address the skin effect that arises at higher frequencies. Table 2.1 shows the skin effect for different frequencies. As can be seen, the skin effect is not present at 50 Hz, but its contribution increases with frequency. Therefore, a hybrid mesh can be used, where the mesh is refined near the edges of the transformer, where the skin effect is most prominent. This will increase the accuracy of the model at higher frequencies. This mesh is shown in fig. 5.1.

Bibliography

- Bizon, M. (2010). *Electricity grid schematic english*. https://commons.wikimedia.org/wiki/File:Electricity_Grid_Schematic_English.svg
- Gebouwd, D. (2008). *Vegeta: Distributietransformator op plantaardige olie*. <https://www.duurzaamgebouwd.nl/artikel/20081218-vegeta-distributietransformator-op-plantaardige-olie>
- Giancoli, D. C. (1995). *Physics*. Prentice Hall.
- N.V., P. A. (2021). *De energietransitie en de financiële impact voor netbeheerders*. <https://www.netbeheernederland.nlnieuws/pwcrapporttijdigeombouwenergiesysteemingevaardoorvoldoendefin>
- Satsangi, S. (2014). “*transformer core market by transformer type (power transformer, distribution transformer, and others) - global opportunity analysis and industry forecast*”. <https://www.alliedmarketresearch.com/transformer-core-market>
- Sudhoff, S. (2014). *Power magnetic devices: A multi-objective design approach* (I. John Wiley & Sons, Ed.) [ISBN: 978-1118824634].
- Sugiyama, M. (2012). Climate change mitigation and electrification. *Energy Policy*, 44, 464–468. <https://doi.org/https://doi.org/10.1016/j.enpol.2012.01.028>
- unknown. (2013). *Magnetic hysteresis loop including the bh curve*. <https://www.electronics-tutorials.ws/electromagnetism/magnetic-hysteresis.html>
- Van der Vorst, A., Rosen, A., Kotsuka, Y., & Djajaputra, D. (2007). Rf/microwave interaction with biological tissues. *Medical Physics*, 34(2), 786–787.
- van Dijk, M., Lahaye, D., Schuddebeurs, J., & van Gijzen, M. (2022). *A theoretical approach towards digital twins: A balance between an empirical and a fundamental model for distribution transformers* [Master Thesis]. <http://resolver.tudelft.nl/uuid:15b25b42-e04b-4ff2-a187-773bc170f061>